KDU Journal of Multidisciplinary Studies (KJMS)
Volume 6. Issue 2 Nov 2024
DOI: https://doi.org/10.4038/kjms.v6i2.149

KJMS 2024 VOL.6 (2): 305-323

EXPLORING ER-UMA TYPE DWARF NOVAE USING PHOTOMETRY DATA OF TRANSITING EXOPLANET SURVEY SATELLITE (TESS)

NI Medagangoda[1], DBTLS Piyadasa[1], MS Abuthahir[1], WMRY Wijesinghe[2] and WIS Fernando[3]

Astronomy Division, Arthur C Clarke Institute for Modern Technologies, Sri Lanka[1]
Department of Physics, University of Sri Jayewardenepura, Sri Lanka[2]
Department of Physics, University of Peradeniya, Sri Lanka[3]

ABSTRACT

An investigation was conducted into eleven ER Ursae Majoris (ER-UMa) star systems using photometric light curve data obtained from the Transiting Exoplanet Survey Satellite (TESS), with a focus on exploring their mass ratios, superoutburst characteristics, and superhump dynamics. This research marks the first instance where all ER Ursae Majoris-type dwarf novae observed by TESS were investigated simultaneously. In this study, we determined the A, B, and C stages of the superhumps in the superoutbursts of each ER-UMa system using the O-C method, and we derived the mean superhump periods as well as the superhump periods in each of the A, B, and C stages. Employing the stage A superhump periods, we estimated the mass ratios (M2/M1) between the white dwarf primary (M1) and the red dwarf secondary (M2) in each system. In addition to the TESS data, we utilised photometric light curve data from the American Association of Variable Star Observers (AAVSO), Zwicky Transient Facility (ZTF), and the All-Sky Automated Survey for Supernovae (ASAS-SN) project to determine variations in supercycle periods and the recurrence periods of normal outbursts for each ER-UMa system.

KEYWORDS: *ER-Ursae Majoris (ER-UMa), Superoutburst, Superhumps, TESS (Transiting Exoplanet Survey Satellite)*

Corresponding Author: NI Medagangoda, Email: Indika.medagangoda@gmail.com

https://orcid.org/0009-0000-0506-073X

1. INTRODUCTION

Nonmagnetic cataclysmic variable stars (CVs) are semi-contact binary systems with a white dwarf primary and a red dwarf secondary. The secondary fills its Roche lobe and transfers mass onto the white dwarf through the inner Lagrange point, forming an accretion disk around it. Among nonmagnetic CVs, Dwarf Novae (DNe) are the most common subtype, with SU Ursae Majoris (SU-UMa) type DNe being one subgroup, alongside U Geminorum (U-Gem) and Z Camelopardalis (Z-Cam) (Warner, 1995).

As explained by (Osaki, 1989), SU-UMa dwarf novae with orbital periods below the period gap (2-3 hours) show two types of outbursts: normal outbursts and superoutbursts. Superoutbursts occur less frequently and last longer than normal outbursts. During superoutbursts, a periodic brightness variation feature known as superhumps can be seen due to the interaction between the orbital period of the system and the precessional period of the disk. The precession is generated by tidal distortion of the elliptical disk caused by a resonance between the orbiting disk particles and the secondary orbit with a 3:1 period ratio (Lasota, 1995).

ER-UMa type dwarf novae, a subset within the SU-UMa type dwarf nova category, distinguish themselves through notably high mass transfer rates and heightened outburst frequencies compared to SU-UMa type members (Kato & Kunjaya, 1995; Kato, *et al*., 1999). Compared to SU-UMa systems, the Supercycle length (the interval between superoutbursts) of ER-UMa systems is narrowed down to 19-48 days (Kato, *et al*., 2013). In other words, short-Supercycle systems (more frequent superoutbursts) within the SU-UMa subgroup are known as ER-UMa DNe (long-Supercycle systems are called WZ Sge stars). The origin of high mass-transfer rate characteristic in the ER-UMa systems with compared to the SU-UMa systems cannot be explained by the canonical view where mass transfer is governed solely by gravitational wave radiation for systems below the period gap (<2h) (Hellier, 2001). Although several possibilities have been suggested for the increased mass transfer in ER-UMa systems other than gravitational wave radiation, the exact reason behind the higher mass transfer rates in ER-UMa systems are yet to be confirmed. In contrast to the usual SU-UMa systems, all ER-UMa systems exhibit large amplitude early superhumps with steady period compared to the normal superhumps (Kato, *et al*., 2013).

A small number of the ER-UMa stars show standstills in their light curves, which are a prominent characteristic in Z Cam type dwarf novae. As described in the disk instability theory, the presence of the standstill may be a result of variable mass transfer (Osaki, 1996), providing some understanding about how the radius and angular moment within the disk vary (Kato & Kojiguchi, 2023). AM CVn stars are known to be Helium rich CVs with compared to the usual CVs which rich in hydrogen. Kato *et al*. (2000) found that CR Boo and V803 in AM CVn category show ER-UMa characteristics in terms of their supercycle period which is 46.3 and ~60 days respectively.

In this context, it is noticeable that various ER-UMa systems show unique characteristics of SU-UMa, Z Cam, and AM CVn dwarf novae categories. This convergence of features across different subclasses of cataclysmic variables points to a more detailed interaction of physical mechanisms than previously understood. These systems might be crucial in bridging the gap between our current models of outbursts mechanisms, disk instability etc. which influence the evolutionary pathways of cataclysmic variables systems. Understanding these unique features could potentially lead to revisions in the theoretical framework that describes the behaviour of such systems.

In this paper, our main focus is to determine whether the observed period changes in superhumps during a superoutburst as described by Kato *et al* (2009) are applicable to determine the mass ratio (q) in the ER-UMa systems, DI UMa, ER-UMa, IX Dra, RZ LMi, V1159 Ori, CM Mic, DDE 48, NY Ser, BK Lyn, BK Lyn, MN Dra and V4140 Sgr obtained via TESS archives. In Section 2, we discuss the acquisition of data for this research, and in Section 3, we present our data analysis and results. Finally, in Sections 4 and 5, we summarise our results and provide a discussion, respectively.

2. METHODOLOGY

Data Acquisition

The main data source used in this research is the archived data of the NASA's Transiting Exoplanet Survey Satellite (TESS). Although the TESS was primarily designed to search transiting exoplanets it produces all-sky survey by using a set of 4 wide-field, red-sensitive cameras (each camera has 4 CCDs) which all together cover with 24 degrees by 96-degree strip of the sky. The TESS exposes these cameras for 2 minutes in each observation and stacks these images for every 30 minutes (Ricker *et al* 2015). TESS observed sky by 26 sectors, mapping the southern half first and the northern half next. TESS data is better than ground-based observational data because it eliminates atmospheric distortions and provides continuous monitoring, enabling the capture of detailed light variations in the targeted systems like dwarf novae. This continuous coverage ensures a more accurate and thorough analysis for this research. TESS data are distributed to the Mikulsky Archive for Space Telescopes (MAST) by the TESS Science Operating Center (SOC). The TESS data comes with two types of light curves which are (1) Simple Aperture Photometry (SAP) flux light curves and (2) Pre-search Data Conditioning SAP (PDCSAP) flux light curves.

For this analysis, only the SAP flux light curve data obtained via MAST were utilized. In the study of Cataclysmic Variables (CVs), the long-term variability captured by SAP flux light curves is crucial for revealing the evolutionary aspects of CVs, making them more suitable for this research compared to PDCSAP light curves.

The analysis in this research included all eleven ER-UMa systems observed by TESS to date, with seven of them demonstrating superoutbursts. For the mass-ratio calculations, these seven systems exhibiting superoutbursts were utilised. Table 01 provides details of the TESS-observed ER-UMa systems.

In addition to utilizing data from TESS, we have obtained photometry light curve data from three supplementary sources: the American Association of Variable Star Observers (AAVSO) (Burbeck, 1917), the Zwicky Transient Facility (ZTF) (Smith *et al*., 2014), and the All-Sky Automated Survey for Supernovae (ASAS), an astronomical survey project (Kochanek *et al*., 2017). These additional datasets are essential for improving the accuracy of determining the supercycle length of ER-UMa systems. While TESS provides high-quality data, it is limited by its relatively short observation period, 27 days, which are insufficient for a comprehensive analysis of objects with longer supercycles, such as ER-UMa systems.

The AAVSO, ZTF, and ASAS datasets extend our observational timeline significantly for 1 year to several decades, allowing us to capture the full range of variability in these systems over much longer periods. By integrating data from these sources, we not only fill in the temporal gaps left by TESS but also increase the robustness of our analysis. This combination of datasets enables us to determine the supercycle lengths with greater precision, enhancing our understanding of the long-term behaviour of ER-UMa systems.

Furthermore, the inclusion of data from multiple independent sources allows for cross-validation of our findings. This redundancy is particularly valuable in astrophysical research, where the ability to confirm results across different datasets strengthens the reliability of the conclusions. The diverse observational techniques and instruments used by AAVSO, ZTF, and ASAS provide different perspectives on the same phenomena, offering a more comprehensive view of the ER-UMa systems' dynamics.

TESS Data Analysis

As mentioned in the section 1, our main objective of this research is to find the applicability of the method introduced by Kato & Osaki (2013) to determine mass-ratio (q) for all ER-UMa systems which were considered. With this purpose we transformed all original SAP flux data into their corresponding magnitudes as follows described in Liu, *et al*., 2024,

$$\Delta\text{mag} = -2.5 \log_{10}(\text{SAP}_{\text{flux}}) + 6 \quad \text{---(1)}$$

The Magnitudes of quiescence part of the light curves were set to 0 to identify the amplitudes of the superoutbursts much easier. (Left panels of Figure 1a & 1b). The trends in superoutbursts of TESS light curves were removed (detrending) by fitting a curve using

Table 01: Details of ER-UMa Stars

Star	TIC ID	Sector	Duration of Observation (Barycentric Julian Date/ BJD 2,457,000+)
DI UMa	279823992	21	1870.44 -1897.79
		47	2579.82-2606.95
ER-UMa	453428902	21	1870.44-1897.79
		48	2607.94-2635.99
		74,75	3312.87-3367.49
IX Dra	236763903	14,15,16	1683.35-1763.32
		18,19	1790.66-1841.15
		21,22	1870.44-1926.49
		24,25,26	1955.79-2035.14
		40,41	2390.65-2446.58
		48,49	2607.93-2664.32
		51,52,53	2692.96-2768.98
		55,56,57	2797.10-2882.11
		60	2936.90-2962.58
		74,75	3312.86-3367.48
RZ LMi	4896794	21	1870.45-1897.79
		48	2607.94-2635.99
V1159 Ori	50620873	32	2174.23-2200.23
CM Mic	91046109	27	2036.28- 2060.65
		67	3126.65- 3154.40
DDE 48	1951569775	41	2419.99-2446.58
		55	2797.10-2824.27
NY Ser	1101183649	24	1955.80-1982.29
		51	2692.96-2717.54
BK Lyn	8765832	21	1870.44-1897.79
MN Dra	236999760	75	3339.78-3367.48
V4140 Sgr	300664897	67	3126.65-3154.40

Locally Weighted Scatterplot Smoothing (LOWESS) method (Cleveland, 1979) to get highlighted the superhump periodic signals in the light curves (Right panels of Figure 1a & 1b). The generalised Lomb–Scargle periodogram (LSP) method (Lomb, 1986; Scargle, 1982; Press & Rybicki, 1989; VanderPlas, 2018) was used to determine the mean superhump periods of each light curves of our sample.

In order to determine q, O-C (Observed minus Calculated) diagrams were constructed for each light curve for our sample using following standard equation,

$$C = t_0 + nP \text{ ---- (2)}$$

Where, t_0 is initial epoch time, n is the cycle number, P is the mean superhump period and C is the calculated time of n^{th} cycle.

The observed values (O) for O-C diagram were obtained using the maximum peak time of each superhump in detrended light curve. The O-C values were then calculated by subtracting the calculated values (C) from the observed (O) values. An O-C graph

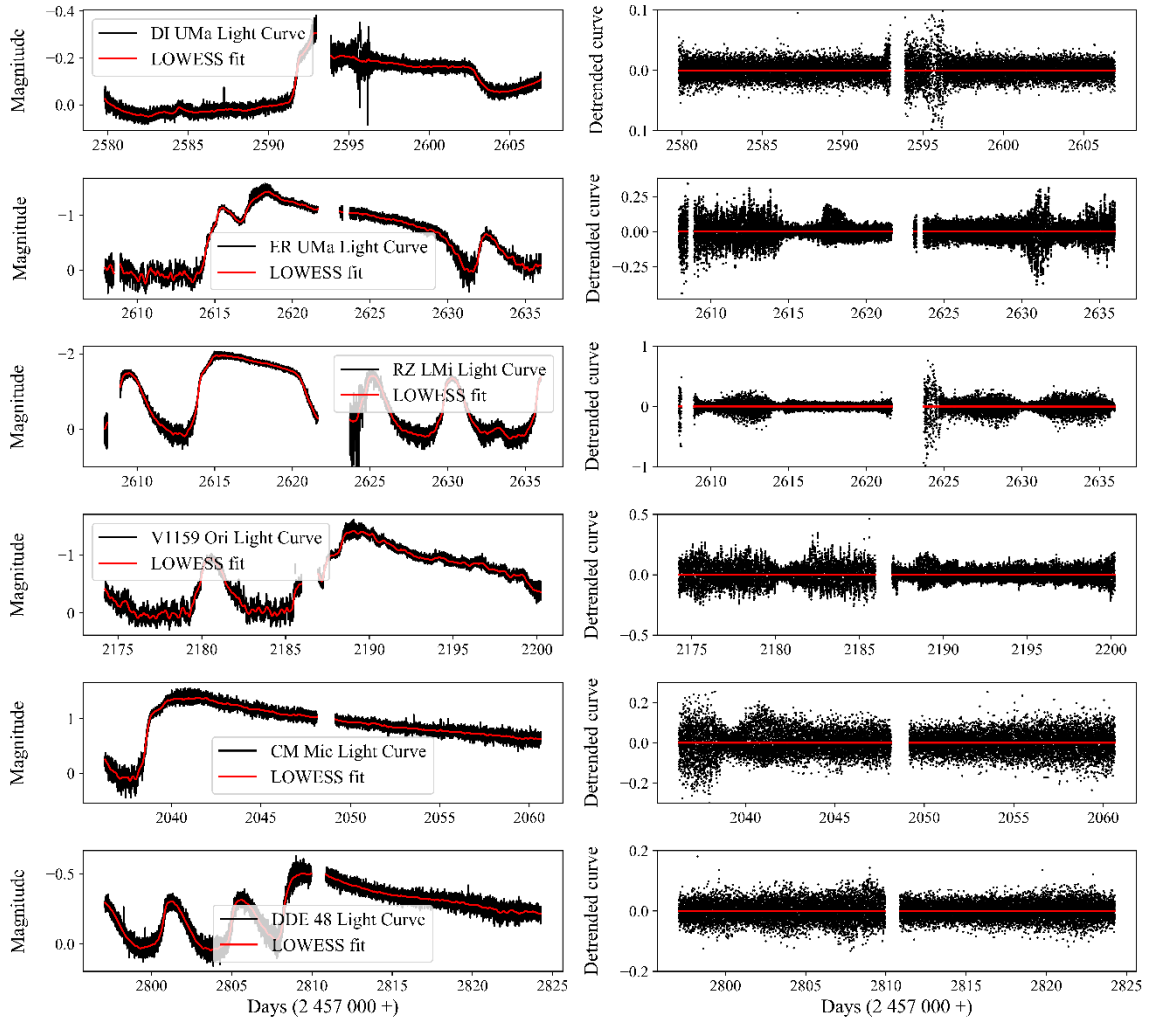

Figure 1a: The left panels show light curves of the superoutbursts of DI UMa, ER-UMa, RZ LMi, V1159 Ori, CM Mic and DDE48. The right panels show detrended light curves of those stars respectively.

was subsequently plotted, displaying the O-C values against the observed peak times. This graph is used to identify any variations that exist in the mean superhump-period within a single superoutburst. Such variations in mean superhump-periods for each superoutbursts are classified by Kato (2009) as three stages: A, B and C.

The Stage A represents the earliest phase of the superhump period variation. The superhumps are growing during this stage and the superhump period is longer than the other stages. During stage A, the superhump amplitude is also reaching its maximum. In the O-C diagram, Stage A is marked by a positive slope, indicating that the observed superhump period is longer than expected. The period derivative $\dot{P}$ (the rate of period change) is positive, which means the period is increasing during this stage. After stage A, the stage B occurs which represents the phase where the superhump period is affected by the unknown disk pressure (Kato & Osaki, 2013). In the O-C diagram, Stage B shows a downward parabolic curve, meaning the O-C values first decrease, reach a minimum, and then increase. However, Stage B has a shorter superhump period than Stage A. The final phase, Stage

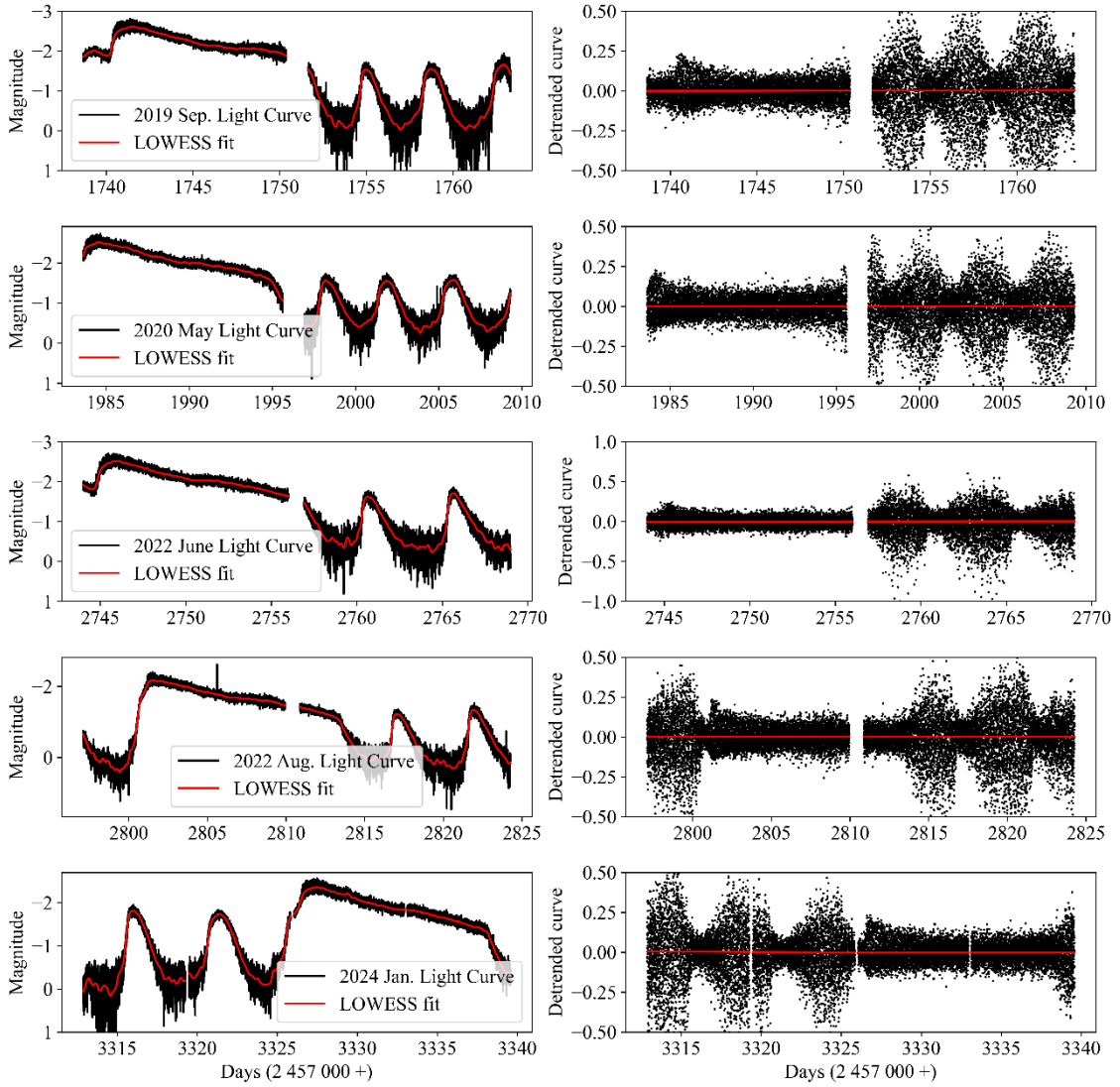

Figure 1b: The left panel shows light curves of the superoutbursts of IX Dra during 2019 September 2020 May 2022 June, 2022 August and 2024 January. The right panel shows detrended light curves of those outbursts respectively.

C superhump period is shorter than in Stage B and typically closer to the orbital period. In the O-C diagram, Stage C is marked by a negative slope, indicating that the observed superhump period is shorter than the expected mean superhump period. The period derivative $\dot{P}$ is negative, meaning the period is decreasing.

After analysing these characteristics, Osaki and Kato (2013) highlighted that, unlike stages B and C, stage A superhumps are unaffected by external forces other than the precession of the disk. As a result, the superhump period in stage A can be utilised more accurately for mass-ratio estimation, expressed as:

$$q = -0.0016 + 2.60\epsilon^* + 3.33(\epsilon^*)^2 + 79.0(\epsilon^*)^3 \text{ --(3)}$$

Where ϵ^* is the fractional superhumps excess in frequency, can be calculated from system's orbital period, P_{orb} and the stage A superhump period, P_{shA} using,

$$\epsilon^* = 1 - P_{orb}/P_{shA}$$

Table 02: Mean Superhump periods and reference orbital periods

Star	Sector	Mean superhump period/days	Error/ days	Orbital period/days
DI UMa	47	0.05532	0.00007	0.054579(6) (Rutkowski, *et al*., 2009)
ER-UMa	48	0.06568	0.00008	0.06366(3) (Thorstensen, *et al*., 1997)
IX Dra	16	0.06706	0.00009	0.06482(3) (Otulakowska-Hypka, *et al*., 2013)
	25	0.06708	0.00008	
	53	0.06697	0.00008	
	55	0.06696	0.00008	
	74	0.06698	0.00008	
RZ LMi	48	0.05949	0.00009	0.05792 (Kato, et al., 2016)
V1159 Ori	32	0.06071	0.00007	0.06217801(13) (Thorstensen, *et al*., 1997)
CM Mic	27	0.08028	0.00010	0.07696(10)

AAVSO, ZTF and ASAS data Analysis

As mentioned, one of the significances that ER-UMa type dwarf novae distinguish themselves is their heightened outburst frequencies (Kato & Kunjaya, 1995; Kato, *et al*., 1999) which fall between 19 days to 48 days, and the normal outbursts on the other hand are packed in a rapid succession between these superoutbursts (Hellier, 2001).

In order to obtain the continuous observation of superoutbursts to determine their supercycle lengths, it is required to obtain older and long-term observational data. For this purpose, AAVSO, ZTF and ASAS photometry archives were used to obtain such data for our ER-UMa sample. The supercycle lengths of each ER-UMa system and the variations in their supercycle periods were determined using those data. The required orbital periods for these calculations were sourced from previously published studies, as the orbital periods of low-inclination (less than 65 degrees) ER-UMa systems cannot be accurately derived from photometric data, such as TESS SAP flux light curves.

3. RESULTS

Results of TESS data analysis

The analysis conducted in this research using TESS photometry data aimed to investigate the mass ratios of ER-UMa systems by analysing the variations in superhump periods. Using the O-C diagrams and mean superhump periods, we identified distinct stages of superhumps and calculated mass ratios. The findings presented below provide the applicability of the method introduced by Kato & Osaki (2013) for ER-UMa systems.

1. Construction of O-C Diagrams:

O-C diagrams (described in Section 2) were constructed for each system to examine any variations in the mean superhump periods. The mean superhump periods were calculated using the generalised Lomb-Scargle (LS) periodogram method, with the required orbital periods obtained from previously published studies (Table 2).

2. Observation of Superhump Stages:

Variations in the mean superhump periods within a single superoutburst were identified as Stage A, B, and C in all O-C diagrams constructed for the sample systems and the Stage demarcations were placed as described in section 2 (see Figure 2). The stages were clearly observed and categorised as per the methodology detailed in Section 2.

Table 03- Superhumps stage A, B, and C period

Star	Sector	Stage	Time period BJD (2 457 000+)	n/ the cycle number	Period/ days	Error/ days
DI UMa	47	A	2592.524-2594.619	0-39	0.05530	0.00015
		B	2594.619-2597.339	40-88	0.05536	0.00010
		C	2597.339-2599.656	89-130	0.05522	0.00011
ER-UMa	48	A	2619.100-2620.047	0-14	0.06614	0.00026
		B	2620.047-2623.140	15-62	0.06592	0.00019
		C	2623.140-2629.222	63-155	0.06547	0.00009
IX Dra	16	A	1740.361-1741.439	0-16	0.06764	0.00024
		B	1741.439-1746.532	17-92	0.06708	0.00011
		C	1746.532-1748.066	93-115	0.06702	0.00019
	25	A	1983.656-1985.204	0-11	0.06707	0.00029
		B	1985.204-1990.847	12-107	0.06706	0.00010
		C	1990.847-1992.706	108-136	0.06656	0.00018
	53	A	2744.789-2746.134	0-20	0.06749	0.00022
		B	2746.134-2751.094	21-94	0.06710	0.00011
		C	2751.094-2754.495	95-145	0.06680	0.00013
	55	A	2800.984-2802.327	0-20	0.06749	0.00022
		B	2802.327-2807.817	21-102	0.06700	0.00011
		C	2807.817-2809.884	103-133	0.06684	0.00017
	74	A	3326.413-3327.756	0-19	0.06746	0.00022
		B	3327.756-3332.450	20-89	0.06714	0.00012
		C	3332.450-3336.120	90-145	0.06681	0.00013
RZ LMi	48	A	2615.038-2615.628	0-10	0.06009	0.00037
		B	2615.628-2619.141	11-69	0.05933	0.00010
		C	2619.141-2620.328	70-89	0.05908	0.00018
V1159 Ori	32	A	2190.927-2191.872	0-15	0.06255	0.00023
		B	2191.872-2194.732	16-62	0.06069	0.00012
		C	2194.732-2199.155	63-135	0.06064	0.00010
CM Mic	27	A	2039.613-2042.759	0-39	0.08084	0.00021
		B	2042.759-2046.292	40-83	0.08049	0.00019
		C	2046.292-2053.028	84-168	0.08008	0.00015

3. Determination of Mean Superhump Periods:

The mean superhump periods for Stage A, B, and C were determined using the LS periodogram method (see Table 3). These stages correspond to different phases within a superoutburst, and the data obtained were critical for subsequent mass-ratio calculations.

4. Mass-Ratio Calculations:

The superhump period in Stage A was specifically used for mass-ratio (q) calculations, as described in Equation (3). The calculated mass-ratio values are provided in Table 4, showing a detailed comparison of the results obtained from this method.

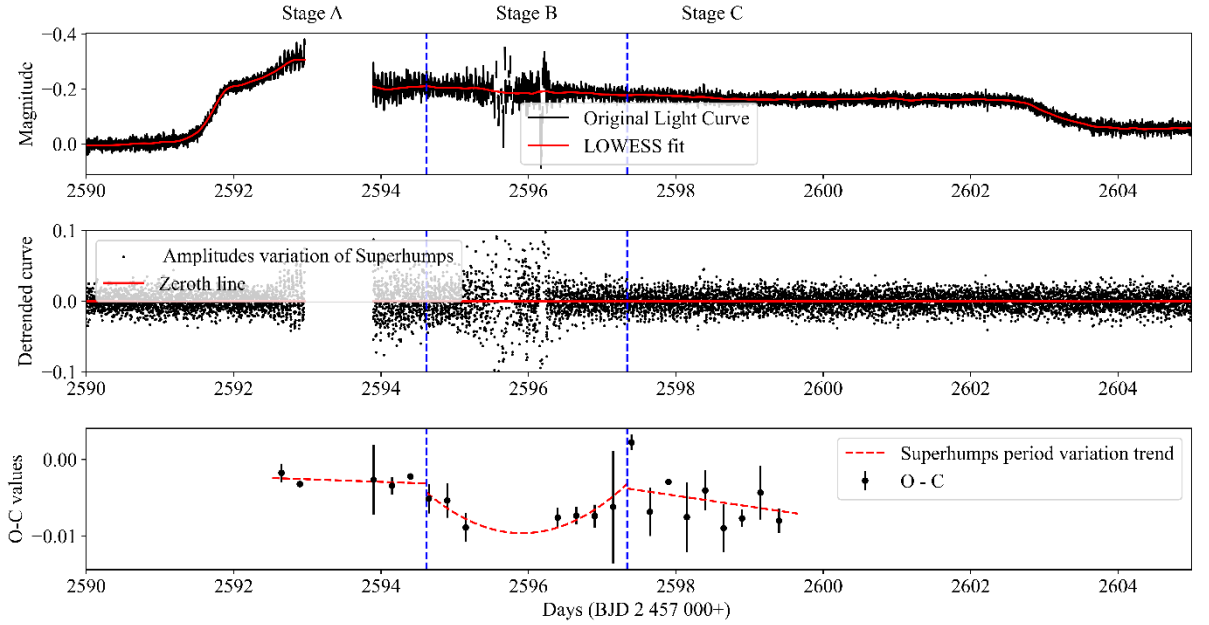

Figure 2a: Top panel shows the light curve of superoutburst of DI UMa. Middle panel shows the detrended light curve. Bottom panel shows the O-C diagram of the superhumps.

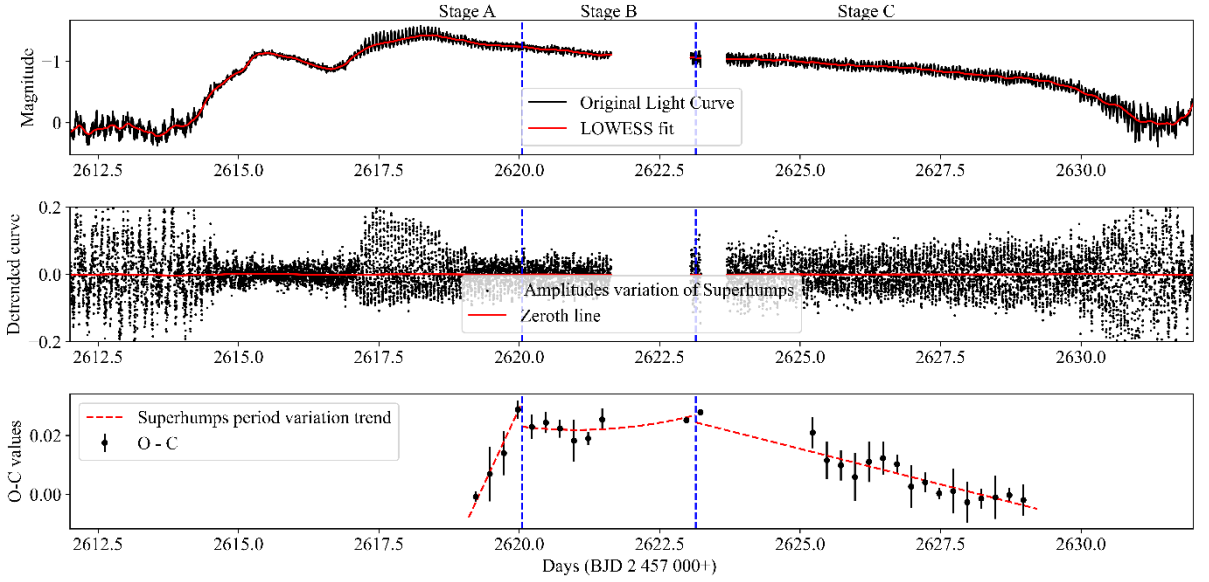

Figure 2b: Top panel shows the light curve of superoutburst of ER-UMa. Middle panel shows the detrended light curve. Bottom panel shows the O-C diagram of the superhumps.

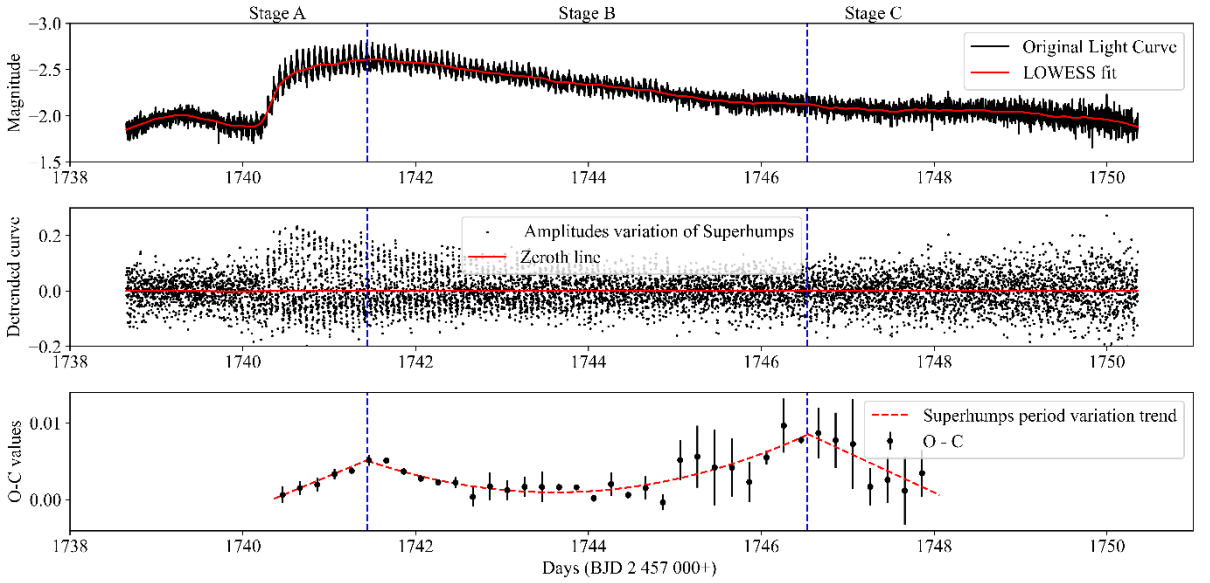

Figure 2c: Top panel shows the light curve of superoutburst of IX Dra (Sector 16). Middle panel shows the detrended light curve. Bottom panel shows the O-C diagram of the superhumps.

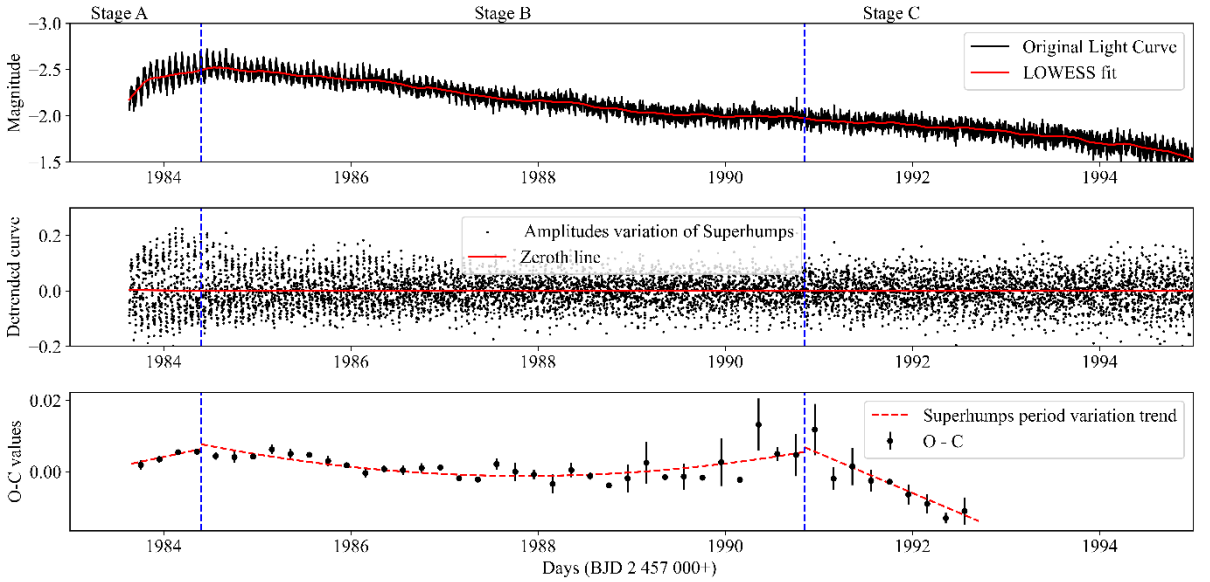

Figure 2d: Top panel shows the light curve of superoutburst of IX Dra (Sector 25). Middle panel shows the detrended light curve. Bottom panel shows the O-C diagram of the superhumps.

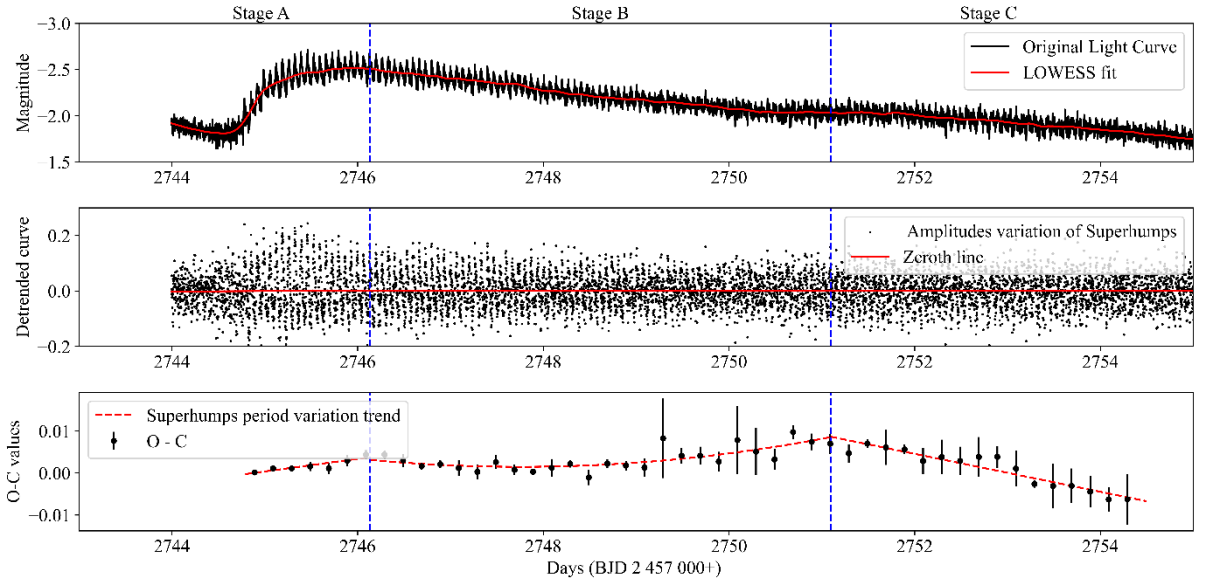

Figure 2e: Top panel shows the light curve of superoutburst of IX Dra (Sector 53). Middle panel shows the detrended light curve. Bottom panel shows the O-C diagram of the superhumps.

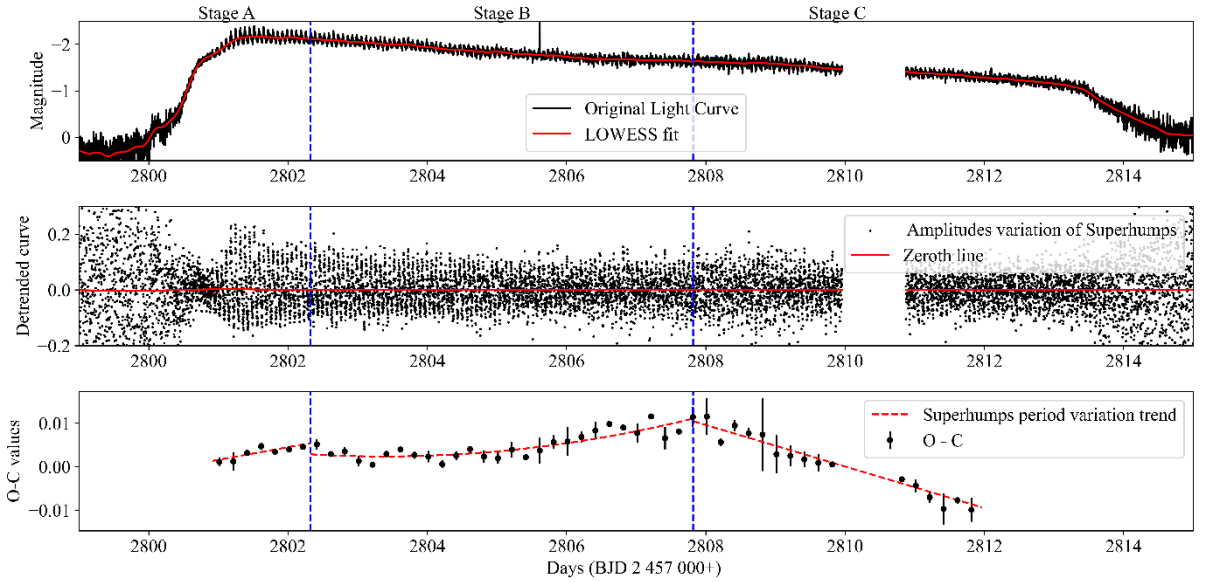

Figure 2f: Top panel shows the light curve of superoutburst of IX Dra (Sector 55). Middle panel shows the detrended light curve. Bottom panel shows the O-C diagram of the superhumps.

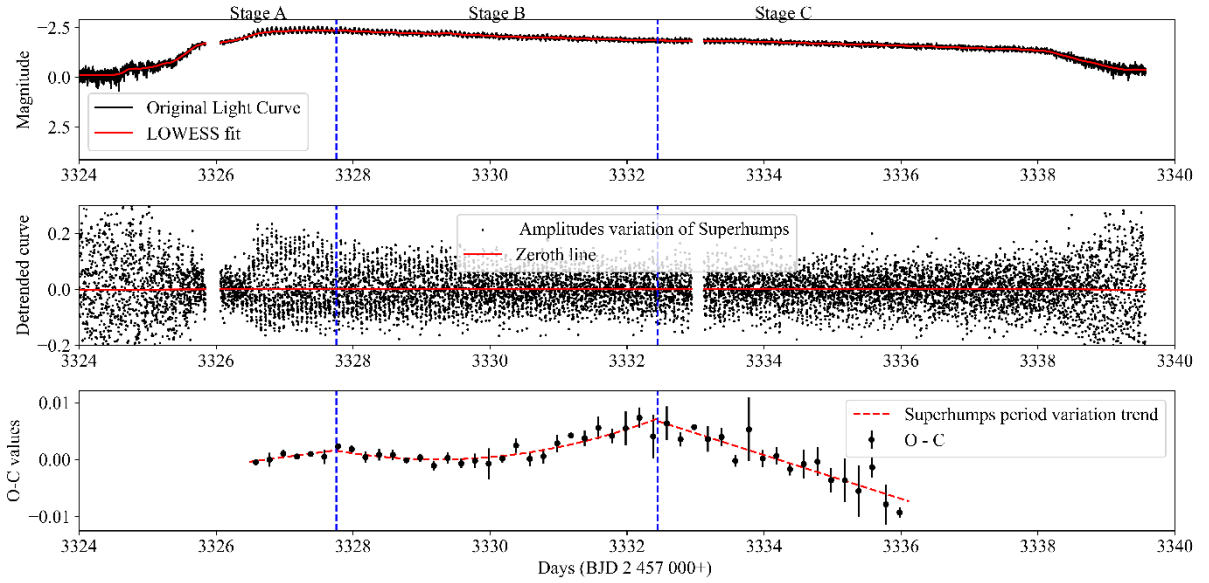

Figure 2g: Top panel shows the light curve of superoutburst of IX Dra (Sector 74). Middle panel shows the detrended light curve. Bottom panel shows the O-C diagram of the superhumps.

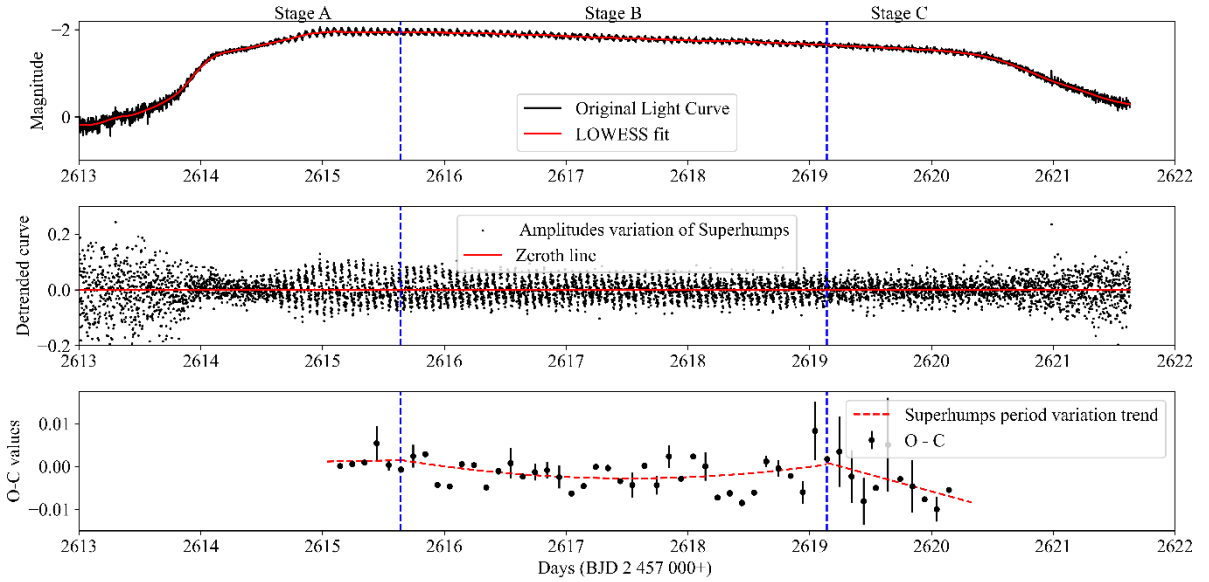

Figure 2h: Top panel shows the light curve of superoutburst of RZ LMi. Middle panel shows the detrended light curve. Bottom panel shows the O-C diagram of the superhumps

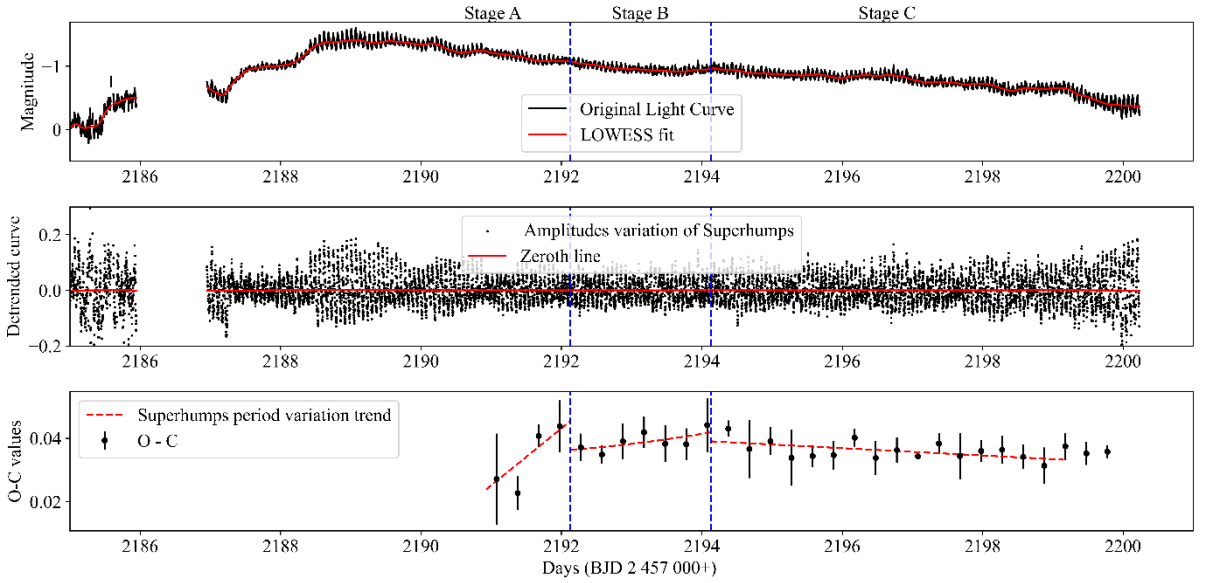

Figure 2i: Top panel shows the light curve of superoutburst of V1159 Ori. Middle panel shows the detrended light curve. Bottom panel shows the O-C diagram of the superhumps.

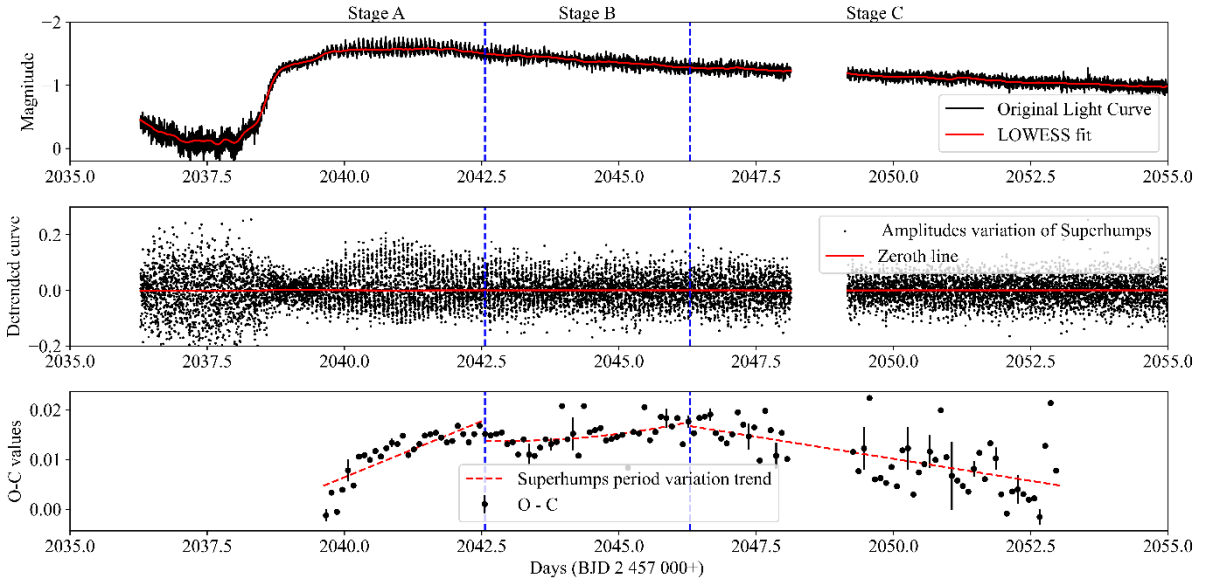

Figure 2j: Top panel shows the light curve of superoutburst of CM Mic. Middle panel shows the detrended light curve. Bottom panel shows the O-C diagram of the superhumps.

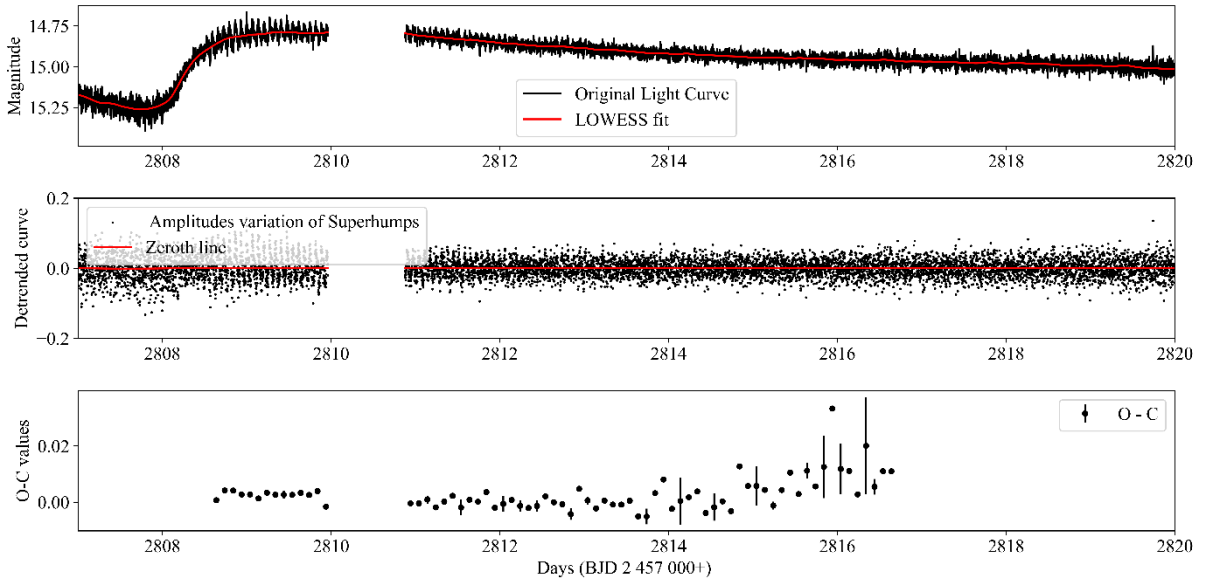

Figure 2i: Top panel shows the light curve of superoutburst of DDE 48. Middle panel shows the detrended light curve. Bottom panel shows the O-C diagram of the superhumps.

Table 4- Mass-Ratio (q) values of stars with and without early large amplitude humps

Star	Mass-Ratio calculated using Stage A superhump period	large amplitude Superhump (LAS) period / days	Mass-Ratio calculated using LAS period	Mass-Ratio calculated from other methods	Percentage deviation (%)
DI UMa	0.033 ± 0.005	No LAS	-	0.06 (Fried, et al., 1999)	45
ER-UMa	0.105 ± 0.010	0.06598	0.097 ± 0.010	0.1 (Ohshima, et al., 2014)	5
IX Dra	0.101 ± 0.015	No LAS	-	0.101 ± 0.009 (Liu & Qian, 2023))	0
RZ LMi	0.100 ± 0.016	No LAS	-	0.105 (Kato, et al., 2016)	4.8
V1159 Ori	0.014 ± 0.009	0.06255	0.014±0.008	No literature data	
CM Mic	0.139 ± 0.030	No LAS	-	No literature data	

5. Comparison with Previous Studies:

Among the ER-UMa systems used for mass-ratio calculations, only ER-UMa and V1159 Ori had mass-ratio values previously determined by other methods. The mass-ratio values obtained in this study are compared with those previously published (see Table 4).

6. Superhump Behaviour in ER-UMa Systems

In certain SU-UMa systems (e.g., RX Vol, SS UMi, V485 Cen), superhumps emerge with a delay after the

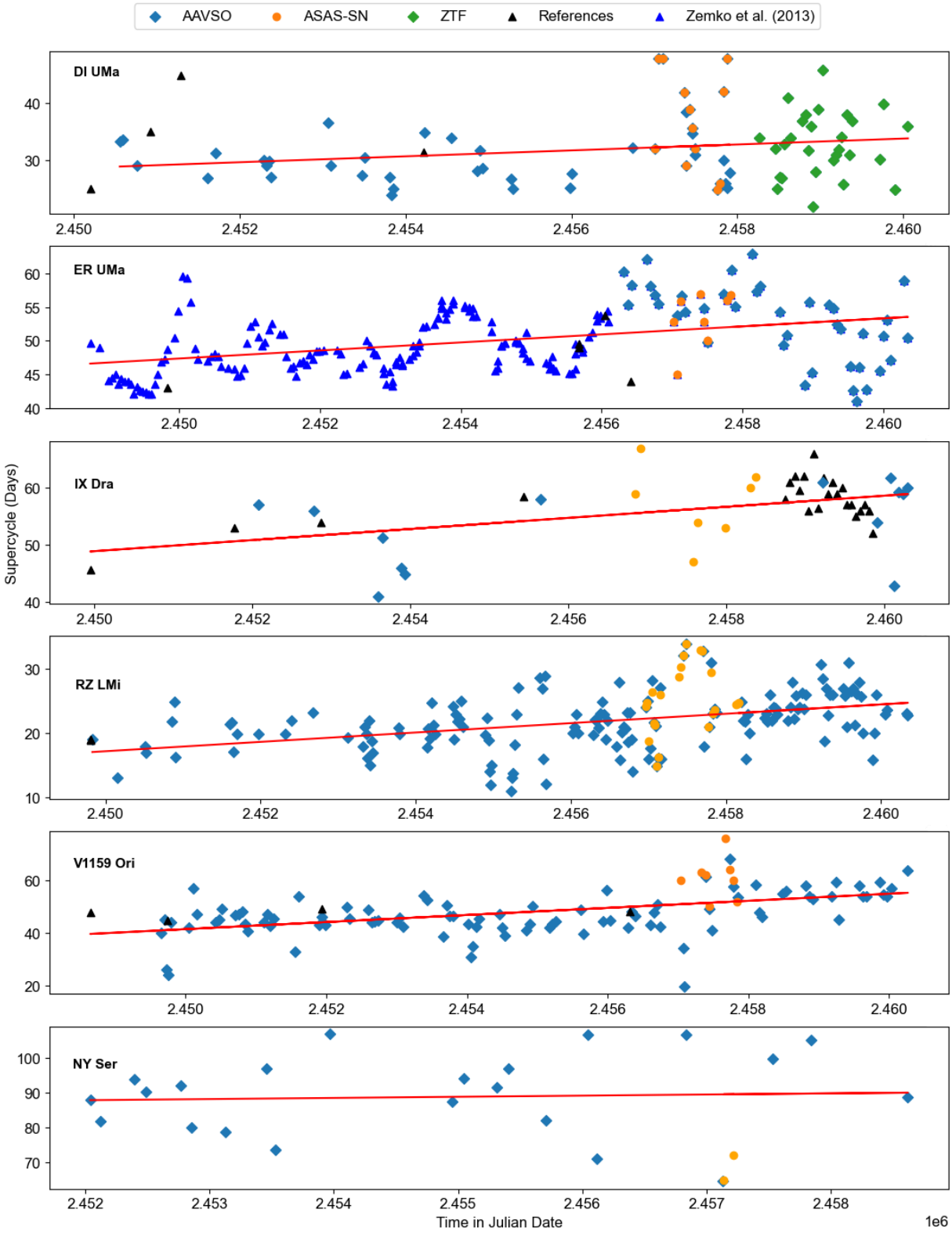

Figure 3: ER-UMa systems supercycle lengths change with time

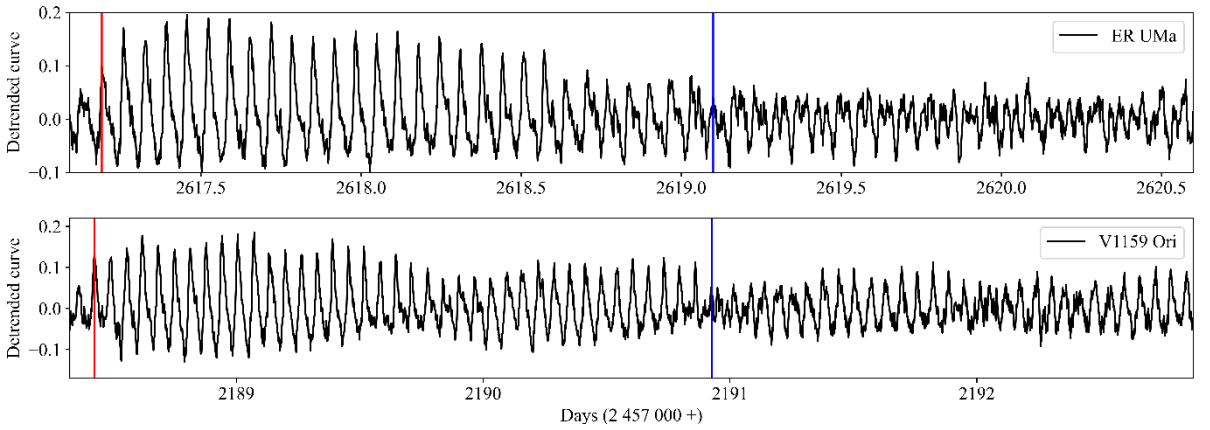

Figure 4: Superhump profiles during the superoutbursts of ER-UMa (top panel) and V 1159Ori (bottom panel). High-amplitude early superhumps are indicated to the left of the blue lines, while normal superhumps are shown to the right of the blue lines.

superoutburst onset, while others (e.g., AK Cnc, GX Cas) show superhumps during the decline phase. In contrast, in the ER-UMa and V1159 Ori systems, superhumps developed during the rise of the superoutburst, with larger amplitudes than in SU-UMa systems (see Figure 4). These high-amplitude superhumps decayed over several days, transitioning to normal-amplitude superhumps. Despite using normal-amplitude superhump periods for mass-ratio calculations, no significant changes in the q values were observed (see Table 4).

Results of AAVSO, ZTF and ASAS data analysis

The supercycle lengths for each ER-UMa system were calculated, and any variations in the supercycle period were tracked over time by plotting the supercycle length against time for each system (see Figure 3).

Our findings suggest that the supercycle period in ER-UMa systems is not static but evolves over time. Table 05 shows the calculated supercycle lengths for each system, along with any detected changes in the supercycle period.

4. DISCUSSION

The ER-UMa systems in our sample exhibit distinctive superhump behaviours that set them apart from SU-UMa type systems, particularly in stars like ER-UMa and V1159 Ori, which display high-amplitude superhumps early in the superoutburst phase. These pronounced superhumps, which gradually transition into the normal-amplitude superhumps typically seen in SU-UMa systems, are likely due to the higher mass-transfer rates in ER-UMa systems (Kato et al., 2013). A high mass-transfer rate causes the accretion disk to expand rapidly, reaching the 3:1 resonance, a critical condition where the orbital period of the disk material matches three times that of the binary system. This resonance induces tidal instabilities within the disk, leading to the precession that generates the characteristic superhump light variations (Warner, 1995). However, not all ER-UMa systems in our sample exhibit these high-amplitude superhumps, even though they also possess higher mass-transfer rates than their SU-UMa counterparts. This indicates that while a higher mass-transfer rate is necessary for the formation of high-amplitude superhumps, it may not be the sole factor. We hypothesise that a threshold range or critical value of mass-transfer rate must be exceeded for these superhumps to manifest with such high amplitude. In systems where this threshold is not met, the superhumps may exhibit lower amplitude. This suggests that superhump formation in ER-UMa systems is governed by a complex interplay of factors, with the mass-transfer rate being a significant, but not exclusive, determinant.

Our analysis underscores the critical role of Stage A superhumps in SU-UMa type systems, particularly in ER-UMa. These superhumps arise when the accretion

Table 05 – Supercycle change rates

System	Observed time duration in JD	Calculated new Supercycle (days)	Calculated Supercycle Change Rate (d d^{-1})	Past Literature Results (d d^{-1})
DI UMa	2450553.7 - 2460057.7	33.78 ± 0.06	5.2×10^{-4}	4.3×10^{-4} (Otulakowska-Hypka & Olech, 2014)
ER-UMa	2456313.0-2460347.4	50.93 ± 0.05	6.0×10^{-4}	1.3×10^{-3} (Otulakowska-Hypka & Olech, 2014) 6.7×10^{-4} (Zemko, et al., 2013) 3.3×10^{-4} (Bean, 2021)
IX Dra	2452085.4-2460296.5	60.78 ± 0.02	9.7×10^{-4}	1.8×10^{-3} (Otulakowska-Hypka & Olech, 2014)
RZ LMi	2449830.5-2460346.8	25.07 ± 0.04	7.3×10^{-4}	5.0×10^{-4} (Otulakowska-Hypka & Olech, 2014) 5.5×10^{-4} (Bean, 2022)
V1159 Ori	2449656.5-2460269.1	55.35 ± 0.02	1.3×10^{-3}	1.1×10^{-3} (Otulakowska-Hypka & Olech, 2014) 3×10^{-3} (Bean, 2022)
NY Ser	2452039.5-2458621.6	-	3.3×10^{-4}	

disk is minimally influenced by external factors, allowing the precession of the disk to be purely dynamical, as noted by Kato & Osaki (2013). This absence of external perturbations makes Stage A superhumps a reliable benchmark for precise mass-ratio calculations. Importantly, our study reveals that the mass-ratio values obtained from Stage A superhumps in ER-UMa and V1159 are in close agreement with those derived from high-amplitude early superhumps. These early superhumps, which occur before Stage A, are similarly devoid of external influences such as pressure effects of the disk, further reinforcing their dynamical nature. The consistency between the mass-ratio values derived from both Stage A and early superhumps supports the reliability of purely dynamical superhumps in mass-ratio determinations, as suggested by Kato & Osaki (2013). To solidify this finding, further investigation is recommended, particularly focusing on higher-amplitude early superhumps in ER-UMa systems, to ensure the robustness of this correlation across a broader range of observations.

Our findings also suggest that the supercycle period in ER-UMa systems is not static but evolves over time. The increase in supercycle length observed in some systems could be indicative of changes in the accretion disk's structure or the mass-transfer rate from the secondary star. According to Osaki's 1995 model, this phenomenon is directly linked to a secular decline in the mass transfer rate between the binary components. The observed lengthening of the supercycle, denoted as Ts, is a direct consequence of this decreasing mass transfer. This trend is indicative of the gradual evolution of the system, potentially leading to a future state where mass transfer is significantly reduced or evolved to another type of binary systems.

However, the variability observed in systems like DDE 48, where the A, B, and C stages of superhumps were not clearly discernible, underscores the complexity of these systems. This could be due to data scattering or other observational challenges, emphasising the need for further research.

5. CONCLUSION

This study investigated the mass ratios and superhump behaviours of ER-UMa systems using TESS photometry data, alongside additional analysis of supercycle periods from AAVSO, ZTF, and ASAS data.

The period of superhumps in Stage A was utilised for mass-ratio calculations. With the exception of the DI UMa system, all calculated mass-ratio values are in good agreement (within 5%) with those obtained through alternative methods, as shown in Table 4. The higher scattering of TESS data for DI UMa, illustrated in Figure 2a, likely explains its deviation (~45%). This finding supports the primary objective of our research: that the method proposed by Osaki & Kato (2013) for determining mass-ratios (q) in binary systems is applicable to ER-UMa type dwarf novae.

Our study also highlighted distinctive superhump behaviours in ER-UMa systems, such as high-amplitude superhumps during the rise of superoutbursts in ER-UMa and V1159 Ori systems. These superhumps transitioned into normal-amplitude superhumps as the superoutburst progressed. Despite this, mass-ratio calculations using both types of superhumps showed no significant changes, further validating the reliability of the Osaki & Kato method.

Additionally, we analysed supercycle periods using data from AAVSO, ZTF, and ASAS, showing that the supercycle length evolves over time. This evolution likely reflects changes in the accretion disk's structure or the mass-transfer rate, consistent with Osaki's (1995) model. The lengthening of the supercycle observed in some systems suggests a gradual decline in mass-transfer rates, indicating an ongoing evolution of these binary systems.

The findings from this study contribute to a more nuanced understanding of the interplay between mass transfer, disk precession, and resonance in dwarf novae. Future work should focus on exploring the mechanisms driving the evolution of supercycle periods and the implications of early high-amplitude superhumps on mass-ratio determination. Additionally, addressing data irregularities and expanding the sample size could help clarify the unique characteristics of ER-UMa type systems.

6. ACKNOWLEDGEMENTS

"This paper includes data collected by the TESS mission, which are publicly available from the Mikulski Archive for Space Telescopes (MAST). Funding for the TESS mission is provided by NASA's Science Mission Directorate."

7. REFERENCES

Bean, S; (2021). Is the supercycle of ER-UMa really increasing? British Astronomical Association Variable Star Section Circular, Jun. pp. 14-17.

Bean, S; (2022). The increasing super-cycle period of V1159 Ori. British Astronomical Association Variable Star Section Circular, Sept. pp.9-12.

Burbeck, A. B; (1917). Meeting of the American Association of Variable Star Observers. *Popular Astronomy*, 25, pp. 413-414.

Cleveland, W. S; (1979). Robust Locally Weighted Regression and Smoothing Scatterplots. *J. of the American Statistical Association*, 74, pp. 829-836.

Fried, R. E. et al; (1999): The Publications of the Astronomical Society of the Pacific. Oct, 111(764), pp. 1275-1280.

Hellier, C; (2001). Cataclysmic Variable Stars: How and why they cary. s.l.:Springer-Praxis.

Kato, T. et al; (2016). RZ Leonis Minoris bridging between ER Ursae Majoris-type dwarf nova and nova-like system. Publications of the Astronomical Society of Japan, 68(6).

Kato, T. & Kojiguchi, N; (2023). CM Mic and other ER-UMa stars showing standstills, s.l.: s.n.

Kato, T. & Kunjaya, C; (1995). Discovery of a Peculiar SU-UMa Type Dwarf Nova ER Ursae Majoris. Publications of the Astronomical Society of Japan, April, 47, pp. 163-168.

Kato, T. et al; (2000). CR Boo: the `helium ER-UMa star' with a 46.3-d supercycle. Jun, 395(1), pp. 140-148.

Kato, T. et al; (1999). Observation of ER-UMa Stars. s.l., Universal Academy Press.

Kato, T. et al., (2013). Observation of ER-UMa Stars, s.l.: s.n.

Kato, T. & Osaki, Y; (2009). New Method of Estimating Binary's Mass Ratios by Using Superhumps. Astronomical Society of Japan, December.Volume 65.

Kato, T. & Osaki, Y; (2013) New Method of Estimating Binary's Mass Ratios by Using Superhumps. Astronomical Society of Japan, December.Volume 65.

Kochanek, C. S. s. b. o. et al; (2017). The All-Sky Automated Survey for Supernovae (ASAS-SN) Light Curve Server v1.0. the Astronomical Society of the Pacific, 129(980).

Lasota, A. e. a; (1995). Superhumps and the 3:1 resonance model. Acta Astronomica, 45, p. 447.

Liu, W. & Qian, S; (2023). Investigation of Superhumps in SU-UMa type Dwarf Novae Based on the Observations. The Astrophysical J., Sept954(2).

Lomb, N. R.; (1986). Least-Squares Frequency Analysis of Unequally Spaced Data. Astrophysics and Space Science, February, 39(2), pp. 447- 462.

Ohshima, T. et al; (2014). Study of negative and positive superhumps in ER Ursae Majoris. Publications of the Astronomical Society of Japan, Jul.66(4).

Osaki, Y; (1989). A model for the superoutburst phenomenon of SU Ursae MAjoris stars. Publications of the Astronomical Society of Japan, 41, pp. 1005-1033.

Osaki, Y; (1996). Dwarf-Nova Outbursts. Publications of the Astronomical Society of Pacific, 108, p. 39.

Otulakowska-Hypka, M. & Olech, A; (2014). Increasing Supercycle Lengths of Active SU-UMa type Dwarf Novae, s.l.: s.n.

Otulakowska-Hypka, M. et al; (2013). IX Draconis - a curious ER-UMa type dwarf nova. Monthly Notices of the Royal Astronomical Society, 429(1), pp. 868-880.

Press, W. H. & Rybicki, G. B; (1989). Fast Algorithm for Spectral Analysis of Unevenly Sampled Data. Astrophysical Journal, March, 338, p. 277.

Ricker, George R; (2015). The Transiting Exoplanet Survey Satellite (TESS): Discovering New Earths and Super-Earths in the Solar Neighborhood, American Astronomical Society, 47(6).

Rutkowski, A. et al; (2009) CURious Variables Experiment (CURVE): CCD photometry of active dwarf nova DI Ursae Majoris. Astronomy and Astrophysics, 497(2), pp. 437-444.

Scargle, J. D; (1982): Studies in astronomical time series analysis. II. Statistical aspects of spectral analysis of unevenly spaced data. Astrophysical Journal, December, Volume 263, pp. 835-853.

Smith, R. M. et al; (2014). The Zwicky transient facility observing system. s.l., s.n.

Thorstensen, J. R., Taylor, C. J., Becker, C. M. & Remillard, R. A; (1997) Orbital Periods for the Unusual Dwarf Novae ER Ursae Majoris and V1159 Orionis. Publications of the Astronomical Society of the Pacific, .109, pp. 477-482.

VanderPlas, J. T; (2018): Understanding the Lomb-Scargle Periodogram. The Astrophysical Journal Supplement Series, 338(1), p. 28.

Warner, B; (1995). Cataclysmic Variable Stars. s.l.:Cambridge University Press.

Zemko, P., Kato, T. & Shugarov, S. Y; (2013). Detection of Change in Supercycles in ER Ursae Majoris. Publications of the Astronomical Society of Japan, June..Volume 65